PAPER

Check for updates

Investigating the role of mixed-cation ionic liquid electrolytes in sodium battery efficiency and stability†

Lixu Huang, [ID] Faezeh Makhlooghiazad, [ID] Luke A. O'Dell, [ID] Patrick C. Howlett and Maria Forsyth*

This study explores the influence of mixed-cation ionic liquid (IL)-NaFSI based electrolyte systems on their physicochemical and electrochemical properties. Utilising two ionic liquids with distinct cation chemistries, (trimethyl isobutyl phosphonium) P_{111i4}^+ and (*N*-methyl-*N*-propylpyrrolidinium) C_3mpyr^+, combined in various ratios with either a constant 42 mol% NaFSI salt concentration or a saturated NaFSI concentration, we examined their thermal behaviour, ionic conductivities, and electrochemical properties over a range of temperatures. We discovered that NaFSI addition disrupts in the neat IL crystallization in both salt concentrations (42 mol% and saturated), resulting in only glass transition temperatures (T_g) that were lower for P_{111i4}/NaFSI than in $C_3mpyrFSI$/NaFSI systems indicating an influence of the cation type on the thermal properties of these IL electrolytes. In both the 42 mol% NaFSI and saturated NaFSI systems, T_g in $C_3mpyrFSI$/$P_{111i4}FSI$/NaFSI mixtures slightly decreased as the $P_{111i4}FSI$ content increased. This was consistent with a slight increase in ionic conductivity and in cation and anion diffusion coefficients with higher $P_{111i4}FSI$ content and temperature. Despite modest changes in ionic conductivity and diffusion coefficients, the electrochemical behaviour shows increased current density and earlier sodium plating initiation with increasing $P_{111i4}FSI$ concentration, highlighting the potential of cation mixing to enhance electrochemical properties suggesting that cation mixing shows potential for improved electrochemical properties through optimized IL electrolyte composition. This work underscores the feasibility of optimizing IL electrolyte compositions for improved performance and stability in sodium batteries, paving the way for future research on cation chemistry effects and practical applications in high-temperature (50 °C) Na−metal-based batteries.

1. Introduction

Fossil fuels, such as coal, petroleum, and natural gas, have long served as the primary global energy sources, driving economic growth but also causing environmental concerns such as the greenhouse effect and climate change. To mitigate these issues, there is an urgent need to transition from fossil fuels to renewable energy sources. Rechargeable batteries emerge as the most competitive option due to their high energy efficiency, low maintenance requirements, and extended cycle life.[1] While lithium-ion batteries currently dominate, their sustainability is challenged by uneven distribution and limited supply of lithium resources, as well as rising prices for related elements

such as cobalt.[2] As an alternative, sodium (Na) batteries present a promising solution for some applications, utilizing abundant and cost-effective sodium resources.[3]

In the current sodium battery research, the focus is mainly on the exploration of positive and negative electrode materials, and electrolyte materials only account for a small proportion of academic discussions.[4,5] Despite the widespread use of commercial organic materials as solvents in electrolytes, their poor thermal stability raises serious safety concerns.[6,7] Therefore, developing safer electrolyte materials has become a key task in promoting the widespread adoption of sodium batteries in energy storage applications. Ionic liquids (ILs), composed of large organic cations and high-charge delocalized anions, present an intriguing alternative.[8] With unique properties such as negligible vapor pressure, low flammability, and high thermal stability, ILs offer safe alternatives to conventional organic electrolytes.[9] An advantage of ionic liquids is that they are designable by the combination of cations and anions, which is also achieved by mixing different ionic liquids

to tune the physicochemical and electrochemical properties of electrolytes.[10]

The most commonly studied ionic liquid electrolytes are predominantly based on imidazolium or pyrrolidinium cations. By making slight modifications to their structure, it is possible to introduce a greater variety of cationic species in ionic liquids than anionic ones. Typically, introducing bulky or long substituents lowers the melting point, while the viscosity increases and the ionic conductivity tends to decrease. As a result, asymmetric cations with short alkyl chains, such as $[C_3mpyr]^+$ and 1-ethyl-3-methylimidazolium $[EMIM]^+$, are often preferred.[3] Compared to their imidazole-based counterparts, non-aromatic pyrrolidine-based cations exhibit greater reductive stability, making them a popular choice for use in lithium and sodium batteries.[11]

The $C_3mpyrFSI$ IL with different molar ratios of NaFSI was characterized by Hagiwara's group, who reported an ionic conductivity of 3.2×10^{-3} S cm^{-1} at 25 °C with an IL:Na ratio of $8:2$.[12] The Na cells with $C_3mpyrFSI$ and 20 mol% NaFSI showed a stable charge–discharge behaviour, delivering capacities of 92 and 106 mA h g^{-1} at 25 and 80 °C, respectively, using a current of 20 mA g^{-1}. Research on the use of different concentrations of NaFSI salt with $C_3mPyrFSI$ has also been systematically conducted by Forsyth et al. They demonstrated that the highest concentration of NaFSI (50 mol% in $C_3mpyrFSI$) showed the most stable Na cycling at higher current densities (1 mA cm^{-2}) relative to the lower concentrations, while the interfacial resistance decreased with high NaFSI salt concentration, as determined by impedance measurements, resulting in faster charge transfer at the interface.[13] Both research groups proposed that the higher transference number for the Na cation in mixtures with higher concentrations of ILs is the reason for the improved performance in Na batteries. This was also recently illustrated by an in-depth modelling study of the dynamics of concentrated IL ions ($C_3mpyrFSI$ + NaFSI) which demonstrated that the structural rearrangement in the IL structure promotes the decoupling motion of Na$^+$ with increasing salt addition.[14,15]

Phosphonium-based ILs and their solid-state counterparts, known as organic ionic plastic crystals (OIPCs), have been reported to offer significant advantages compared to their nitrogen-based IL correspondents. These advantages include higher ionic conductivity and enhanced electrochemical stability.[16] Hilder and co-workers explored the physicochemical and electrochemical properties of FSI$^-$ anion-based ILs paired with three different cations: two small alkyl phosphonium cations: P_{111i4}^+ and $P_{1i4i4i4}^+$ and an alkoxy ammonium counter cations: $N_{2(2O2O1)3}^+$. These ILs were mixed with NaFSI salt to near saturation (at approximately $1:1$ mol ratio). At 50 °C, the ionic conductivity of the high salt content IL mixture ($P_{111i4}FSI$–NaFSI) was measured to be 4.4 mS cm^{-1} which is the highest among the electrolytes studied, whereas the $N_{2(2O2O1)3}FSI$–NaFSI system exhibited the lowest ionic conductivity. Interestingly, despite its lower ionic conductivity, the $N_{2(2O2O1)3}$-FSI–NaFSI mixture demonstrated excellent reversible sodium reduction/oxidation in CV measurements, with a maximum

peak current density of 10 mA cm^{-2}, comparable to 17 mA cm^{-2} of the $P_{111i4}FSI$–NaFSI system, which had the highest ionic conductivity. Na symmetric cycling revealed that sodium stripping/plating in the $N_{2(2O2O1)3}FSI$–NaFSI mixture was as stable as in the $P_{111i4}FSI$–NaFSI electrolyte underscoring the critical role of the solid–electrolyte interphase (SEI) structure and morphology on the surface of sodium metal in cycling performance. Rakov et al. reported the formation of a Na$_x$(FSI)$_y$ molten salt-like nanostructured interfacial layer at the surface of the electrode, preconditioned with a high-current-density protocol in a high sodium salt content $C_3mpyrFSI$ electrolyte containing 50 mol% NaFSI.[17] In a comparative surface study, Ferdousi et al. highlighted that phosphonium IL-based electrolytes demonstrated higher cycling stability and capacity (up to 4 mA h cm^{-2} at current densities of 1, 2, and 4 mA h cm^{-2}) compared to the rapid failure of $C_3mpyrFSI$ electrolytes (at 1 mA h cm^{-2} for 4 mA h cm^{-2}). Surface characterization revealed that the addition of water significantly improved the SEI of the phosphonium cation IL, evidenced by a greater proportion of a Na complex and a NaF-rich surface compared to that with $C_3mpyrFSI$.[18]

It has been reported that the properties of ILs, such as ionic conductivity, viscosity, and cost, can be adjusted by mixing ILs with different anions. The addition of NaDCA, NaFTFSI, NaTFSI and NaFSI influences the morphology of the Na surface after cycling in $C_3mpyrDCA$ IL. NaFSI was found to form a more stable SEI layer, as indicated by prolonged symmetrical cell cycling. In contrast, both the TFSI and FTFSI salts led to the formation of thicker, highly passivating surfaces. The SEI layer in the $C_3mpyrDCA$–NaFSI system was primarily composed of NaF, which facilitated stable cycling with the lowest overpotential for more than 100 cycles.[19]

This study demonstrated that, in principle, utilizing a low-cost IL can retain the benefit of safety and recyclability while simultaneously providing the desirable SEI forming features required for effective battery cycling. While most research has focused on the effect of mixed anion ILs on Na anodes, only minimal attention has been given to the effect of mixed cations and the implications on bulk properties and electrochemical behaviour.

In this study, we investigate the influence of mixed-cation IL electrolyte systems on their physicochemical and electrochemical properties, focusing on P_{111i4}^+ and C_3mpyr^+ as cation chemistry. P_{111i4}^+ is recognized for its high ionic conductivity and chemical electrochemical stability; however, its synthesis pathway results in high cost which would currently limit its practical application. Conversely, C_3mpyr^+ emerges as a more cost-effective alternative with promising properties. By mixing these ILs, we aim to achieve a balance between superior performance and economic feasibility. We select the FSI$^-$ anion for its ability to form a reliable solid electrolyte interphase (SEI). Our methodology involves two strategies: initially, mixing varying ratios of $C_3mpyrFSI/P_{111i4}FSI$ with a saturated NaFSI to maintain a high salt concentration, beneficial for uniform metal deposition and dendrite prevention on the metal anode during cycling. Second, we employed a fixed 42 mol% NaFSI

concentration – saturated in the $P_{111i4}FSI$ IL – to isolate the effects of cation chemistry on the mixed IL electrolyte's properties. Our findings reveal a direct correlation between $C_3mpyrFSI$ proportion and physicochemical properties in the 42 mol% NaFSI system, as well as the significant impact of sodium salt concentration on these properties.

2. Experimental and/or theoretical methods

2.1. Sample preparation

Ionic liquids $P_{111i4}FSI$ and $C_3mpyrFSI$ were purchased from Boron Molecular company with 99.9% purity, and sodium bis(fluorosulfonyl)imide (NaFSI, 99.9%) was purchased from Solvionic with 99.9% purity. The structures of the two ionic liquids are presented in Fig. S1 (ESI†). To eliminate the effect of water, the two ILs were dried at 50 °C under vacuum for 48 hours and their water content was reduced to less than 50 ppm as confirmed by Karl Fischer methods (831 Karl Fisher Coulometer with Hydranal® Coulomat AG as the titrant). As shown in Table 1, $C_3mpyrFSI$ and $P_{111i4}FSI$ were mixed at different ratios, and NaFSI salt was added until near saturation, all within an argon-atmosphere glove box. Finally, all electrolytes were vacuum-sealed and stored in sealed vials under argon inside the glove box.

$C_3mpyrFSI$ and $P_{111i4}FSI$ were also mixed at different ratios, and a fixed NaFSI concentration (42 mol%) was added as shown in Table 2.

2.2. Differential scanning calorimetry (DSC)

DSC measurements were conducted to investigate the thermal behaviour of the electrolytes, such as melting temperature, glass transition temperature, transition entropies and enthalpies. The instrument used for DSC was a NETZSCH DSC 214 Polyma. Three heating and cooling cycles were performed at a scan rate of 10 °C min⁻¹ from −120 to 30 °C. The first scan was

Table 1 Electrolyte composition with the saturated NaFSI system

	Electrolyte composition (mol%)		IL composition (mol%)	
Expt. no.	NaFSI salt	ILs	$C_3mpyrFSI$	$P_{111i4}FSI$
1	50	50	100	0
2	49	51	75	25
3	47	53	45	55
4	45	55	15	85
5	36	64	0	100

Table 2 Electrolyte composition with 42 mol% NaFSI system

	Electrolyte composition (mol%)		IL composition (mol%)	
Expt. no.	NaFSI salt	ILs	$C_3mpyrFSI$	$P_{111i4}FSI$
1	42	58	100	0
2	42	58	80	20
3	42	58	50	50
4	42	58	20	80
5	42	58	0	100

affected by the thermal history of the sample; therefore, the reproducible data from the second and third scans are reported. The onset temperature was taken as the glass transition temperature. Cyclohexane from Sigma Aldrich was used as an analytical standard for temperature correction.

2.3. Ionic conductivity

A BioLogic MTZ-35 impedance analyzer was used to determine ionic conductivity through EIS measurements. In this study, a custom-built dip-cell was used for conductivity measurements of the electrolyte solutions. This cell contained two platinum wires sheathed in glass sealed with a rubber O-ring and fitted into the cavity of a brass block that was connected to a Eurotherm 2204 temperature controller. Temperature ramping was set at 0.5 °C min⁻¹ until the desired temperature was obtained (±0.3 °C for 20 min). Electrolyte resistivity was determined from the touch down point of the Nyquist plot (x-axis). This resistance was used to calculate conductivity by eqn (1).

$$R = \frac{1}{\sigma}\frac{l}{A} = G^* \times \frac{1}{\sigma} \tag{1}$$

where R is the resistance of the electrolyte from the Nyquist plot in Ω, σ is the conductivity in S cm⁻¹ and G^* is the cell constant, as obtained by measuring the cell resistance of a standard reference solution of known conductivity (eqn (2)). After measuring cell constant and resistance of the electrolyte solution, conductivity of the solution can be calculated from eqn (3). The results are presented on a logarithmic scale.

$$G^* = R \times \sigma \tag{2}$$

$$\sigma = \frac{G^*}{R} \tag{3}$$

A standard solution, 0.01 M KCl, was used to calculate the cell constant at 30 °C. Frequency range was 10 MHz to 1 Hz with a voltage amplitude 0.1 V over the temperature range of −20 to 120 °C. Output data were graphically expressed as Bode or Nyquist plots; Nyquist plots, which present the imaginary part of the impedance vs. the real impedance, were used in this study.[20] Electrolyte resistivity was determined from the touch down point of the Nyquist plot (x-axis).

2.4. Nuclear magnetic resonance spectroscopy (NMR) and ion diffusion measurements

Pulsed-field gradient stimulated echo (PFG-STE) diffusion measurements were conducted for ¹H, ¹⁹F, and ³¹P using a Bruker Avance III 500 MHz wide-bore spectrometer equipped with a 5 mm PFG probe. The gradient pulse time (δ = 2 ms) and the diffusion time (Δ = 20 ms) were employed, following the procedure described by Bayley et al.[21] The diffusion coefficients for the C_3mpyr^+ cation, the FSI^- anion, and the P_{111i4}^+ cation were determined using the respective ¹H, ¹⁹F, and ³¹P nuclei. Sodium diffusion could not be obtained due to the short relaxation time of the ²³Na nucleus in these samples. To minimize the effects of convection, the samples were filled to a height of 50 mm in 3 mm NMR tubes within an argon-filled glovebox, flame-sealed, and then water-bathed inside 5 mm

NMR tubes sealed with Teflon tape and a cap. The temperature range for these experiments spanned from 20 to 80 °C.

2.5. Cyclic voltammetry

Cyclic voltammetry (CV) experiments were conducted using a Biologic VMP3 potentiostat with a coin cell setup. The coin cells (components CR2032) were purchased from Hoshen Corporation, Japan. The working electrode is made of copper (12.7 mm diameter), and the counter and pseudo-reference electrode is made of sodium metal (8 mm diameter). The copper electrode was punched and washed with 1 M HCl solution for 2 minutes followed by washing with deionized (DI) water for 2 minutes and finally with acetone for 2 minutes. The electrodes were then vacuum-dried for 24 hours at 100 °C and transferred into the glovebox. A 16 mm diameter polyethylene separator (gratis, Lydall, 7P03A, 50 mm thickness, 85% 0.3 mm porosity) soaked with the electrolyte solution was used. A 0.5 mm spacer and a 1.4 mm spring were used to ensure contact. All the measurements were carried out at 50 °C and at a scan rate of 20 mV s^{-1}. The onset potential was determined by intersection of the tangent to the exponentially increasing current part of the current curve with the linear extrapolation of the baseline current.

3. Results and discussion

3.1. Mixed cations with a saturated NaFSI system

The utilization of a high salt concentration in the electrolyte proves beneficial in achieving uniform metal deposition and preventing dendrite formation at the metal anode during cycling, as reported in previous studies.[17] Consequently, we initially chose the saturation salt concentration for each of the mixed IL electrolytes to compare what we considered to be the optimum salt composition in each case. From the literature, the saturation limits of NaFSI in pure P_{111i4}FSI and C_3mpyrFSI are reported to be 42 mol% and 50 mol%, respectively.[16,22] Results from solubility tests showed that the saturation limit of NaFSI in 15:85, 45:55, and 75:25 C_3mpyrFSI:P_{111i4}FSI was measured to be 45 mol%, 47 mol%, and 49 mol%, respectively. The properties of these systems were initially investigated.

3.1.1. Thermal behaviour and ionic conductivity measurements. Fig. 1 displays the DSC traces of P_{111i4}FSI and C_3mpyrFSI, both in combination with saturated NaFSI, where we have P_{111i4}FSI with 42 mol% NaFSI and C_3mpyrFSI with 50 mol% NaFSI, as well as mixtures of mixed ILs along with saturated NaFSI. The DSC heating traces of the pure ILs reveal endothermic transition at 12.3 °C for P_{111i4}FSI and melting transitions at −5 °C for C_3mpyrFSI.[23,24] However, upon the addition of saturated NaFSI to the pure ILs, only glass transitions (T_g) at −65.96 °C (onset) for C_3mpyrFSI and −74.95 °C (onset) for P_{111i4}FSI were observed. This suggests that the addition of NaFSI disrupts the crystallization process in these ILs.

In cases where mixed ILs with various ratios were combined with saturated NaFSI, only T_gs were detected. Notably, the onset
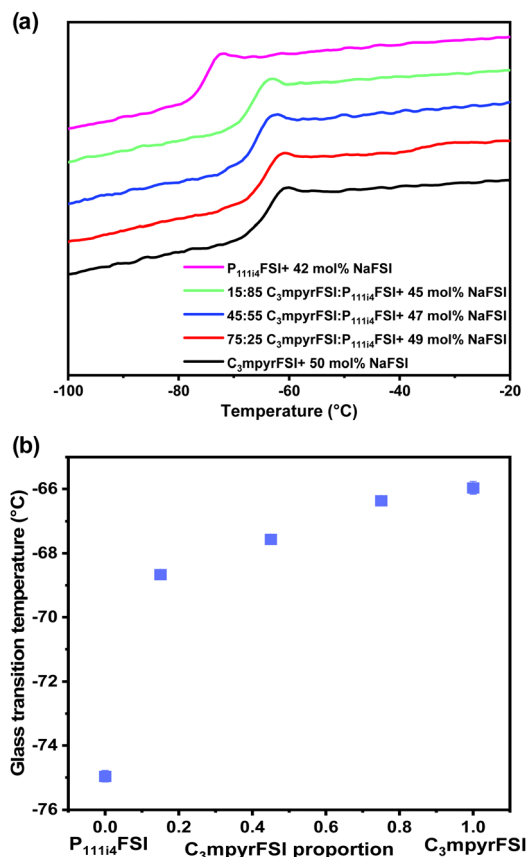

Fig. 1 (a) DSC heating traces of the mixed P_{111i4}FSI and C_3mpyrFSI with a saturated NaFSI system. (b) Glass transition temperature as a function of C_3mpyrFSI proportion.

of these T_gs increases with higher C_3mpyrFSI content, which also contains higher salt content. Specifically, a significant increase in T_g was observed when the content of C_3mpyrFSI increased from 0 to 15 mol% from −74.95 °C to −68.66 °C. The thermal behaviour of the mixtures is more similar to that of C_3mpyrFSI even with only 15 mol% of C_3mpyrFSI in the mixture. Interestingly, ΔT_g (the temperature range between the onset and end of the T_g peak) is larger for the neat P_{111i4}FSI IL indicating less fragility of this IL compared to both C_3mpyrFSI and mixtures of the two ILs.[25] The ion mobility in the mixtures is discussed in the following sections.

The ionic conductivity of the mixtures as shown in Fig. 2 increases with the addition of P_{111i4}FSI to the C_3mpyrFSI system. In the lower temperature ranges (−20 to 0 °C), adding 25% P_{111i4}FSI significantly increases the ionic conductivity of the neat C_3mpyrFSI/NaFSI system. Here, P_{111i4}FSI emerges as the dominant contributor to the enhancement of the ionic conductivity, as the mixtures exhibit ionic conductivities more closely aligned with those of pure P_{111i4}FSI as illustrated in Fig. 2b.

At higher temperatures (above 0 °C), the trend in ionic conductivity appears nearly linear as depicted in Fig. 2c and d. It is noteworthy that the increase in ionic conductivity could be due to either a reduction in NaFSI salt concentration, which lowers the viscosity, or an increased proportion of P_{111i4}FSI, as
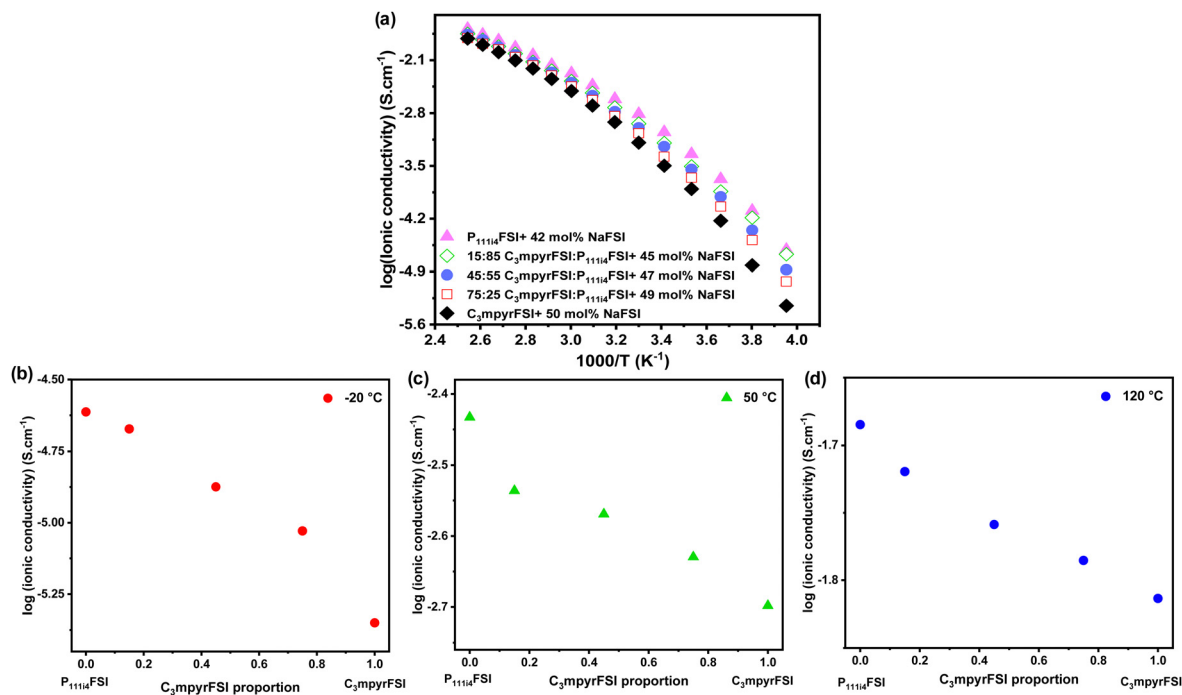
Fig. 2 (a) Temperature-dependent ionic conductivity, (b) the ionic conductivity at −20 °C, (c) the ionic conductivity at 50 °C, (d) the ionic conductivity at 120 °C.

the NaFSI salt concentration was increased from 42 mol% in P_{111i4}FSI to 50 mol% in C_3mpyrFSI.

3.1.2. Diffusion coefficient. In addition to the ionic conductivity of the electrolytes, NMR spectroscopy and pulsed field gradient diffusion measurements were used to characterize the mobility of individual ionic species as a function of temperature and composition. The diffusion of FSI^- was measured using ^{19}F PFG-NMR. The diffusion of C_3mpyr$^+$ was measured
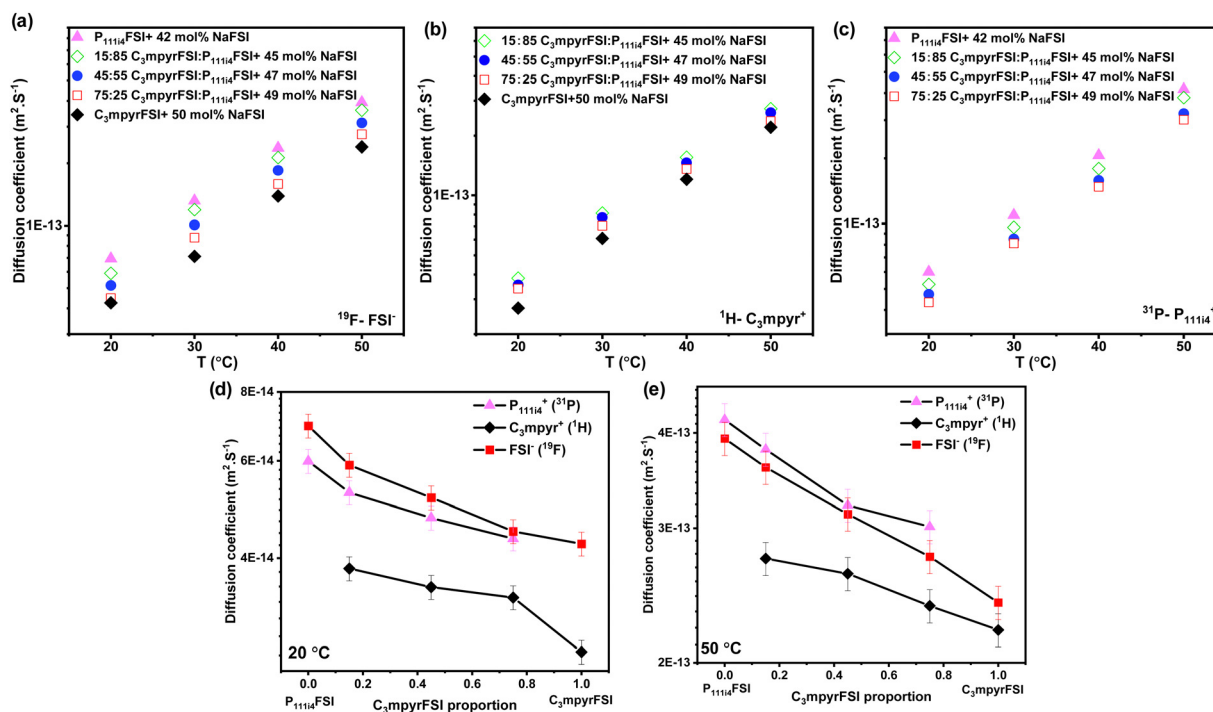

Fig. 3 Diffusion coefficients of (a) anion (^{19}F), (b) C_3mpyr cation (^1H), (c) P_{111i4} cation (^{31}P) as a function of C_3mpyrFSI proportion, (d) diffusion coefficients at 20 °C (e) at 50 °C.

with ^{1}H NMR, while P_{111i4}^+ was measured through ^{31}P NMR. This approach was necessary because as demonstrated in Fig. S3 (ESI†), C_3mpyr$^+$ exhibits distinct peak positions (3.2–2.2 kHz) while all peaks from P_{111i4}^+ are overlapped in the ^{1}H NMR. Therefore, ^{31}P PFG-NMR was used to measure the diffusion of P_{111i4}^+. ^{23}Na diffusion in these samples could not be measured due to the very short transverse relaxation time (T_2).

Fig. 3 presents the diffusion coefficients of ions as a function of the C_3mpyrFSI proportion within the temperature range of 20 to 50 °C. Fig. 3a–c show a consistent increase in the diffusion coefficients for both cations and anions with higher P_{111i4}FSI content and higher temperature. These trends correspond to the observed decrease in glass transition temperature and ionic conductivity. The anion diffusion coefficient is slightly higher than that of the cation. This is likely due to the anion's smaller size, which may allow it to diffuse faster. Fig. 3d and e depict almost linear trends in the diffusion coefficients for cations and anions as the C_3mpyrFSI proportion changes. A significant observation is a distinct drop in the diffusion coefficient of C_3mpyr$^+$ at 20 °C.

Three-electrode cyclic voltammetry was employed to characterize the electrochemical properties of the electrolytes, as shown in Fig. 4, using a Cu working electrode which has previously been reported to facilitate plating/stripping of sodium metal.[19,26] The current density of the reduction peak follows the ratio of two mixed ILs, C_3mpyrFSI $<$ 75:25 C_3mpyrFSI:P_{111i4}FSI $<$ 45:55 C_3mpyrFSI:P_{111i4}FSI $<$ 15:85 C_3mPyrFSI:P_{111i4}FSI $<$ P_{111i4}FSI. At the same potential, the higher current density is likely associated with a lower overall resistance (including bulk electrolyte, charge transfer and SEI resistance). The P_{111i4}FSI certainly has the highest ionic conductivity in the bulk and has previously been suggested to have an improved SEI.[18] The current density of the mixtures are closer to the value for C_3mpyrFSI, possibly due to the closer ionic conductivity of the mixtures to C_3mpyrFSI at 50 °C and may also reflect the dominance of the C_3mpyr cation on the interfacial properties. The enlarged reduction process
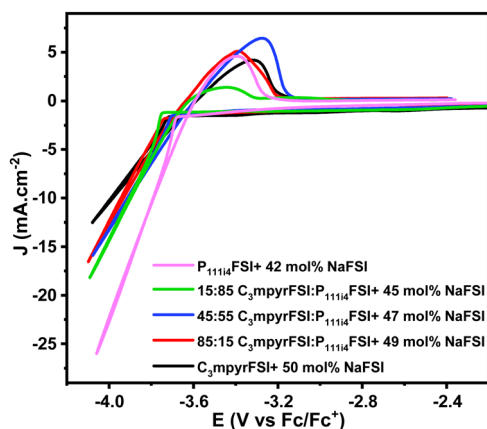

Fig. 5 (a) Thermal phase behaviour of the mixed P_{111i4}FSI and C_3mpyrFSI with 42 mol% NaFSI system. (b) Glass transition temperature as a function of C_3mpyrFSI proportion.

presented in Fig. S4 (ESI†) shows the reductive decomposition of the electrolyte which is also dependent on the electrolyte composition and appears to be more extensive in the C_3mpyrFSI case.

3.2. Mixed cations with a constant concentration of NaFSI (42 mol%)

As the saturated system involves two variables – the cation ratio and the NaFSI salt concentration – the specific influence of the cation ratio on the physicochemical properties remains uncertain. To investigate the impact of cations on both physicochemical and electrochemical properties, a fixed NaFSI concentration (42 mol%) system was used.

3.2.1. Thermal behaviour and ionic conductivity measurements.
Fig. 5a shows the thermal behaviour of the mixed P_{111i4}FSI and C_3mpyrFSI system, at various ratios, with 42 mol% NaFSI. There is only a glass transition peak at −70.26 and −74.95 °C (onset), in the C_3mpyrFSI/NaFSI and P_{111i4}FSI/NaFSI systems, respectively. In the ternary systems of C_3mpyrFSI:P_{111i4}FSI with 42 mol% NaFSI, the glass transition temperature (T_g) rises slightly with increasing C_3mpyrFSI content from −74.2 °C at 20 mol% C_3mpyrFSI to −71.5 °C in 80 mol%

Fig. 4 Cyclic voltammetry curves for the mixed P_{111i4}FSI and C_3mpyrFSI with a saturated NaFSI system during the 1st cycle.
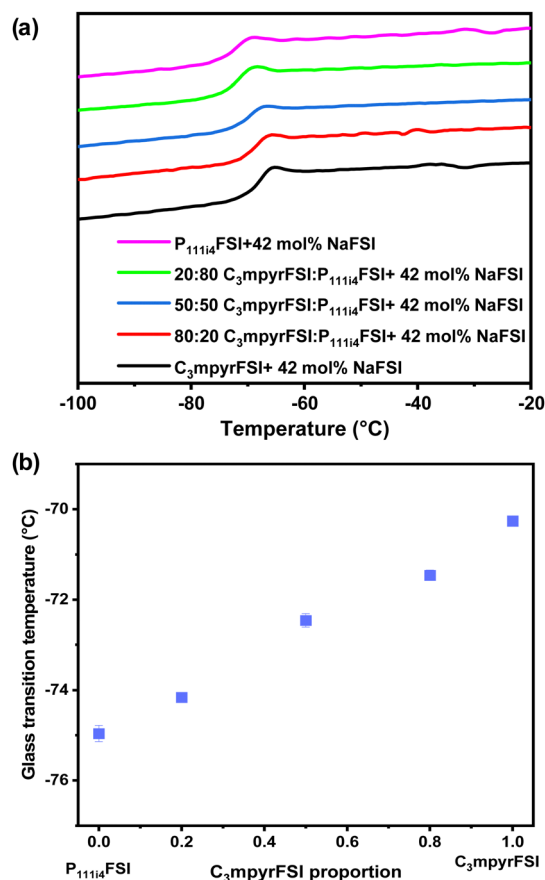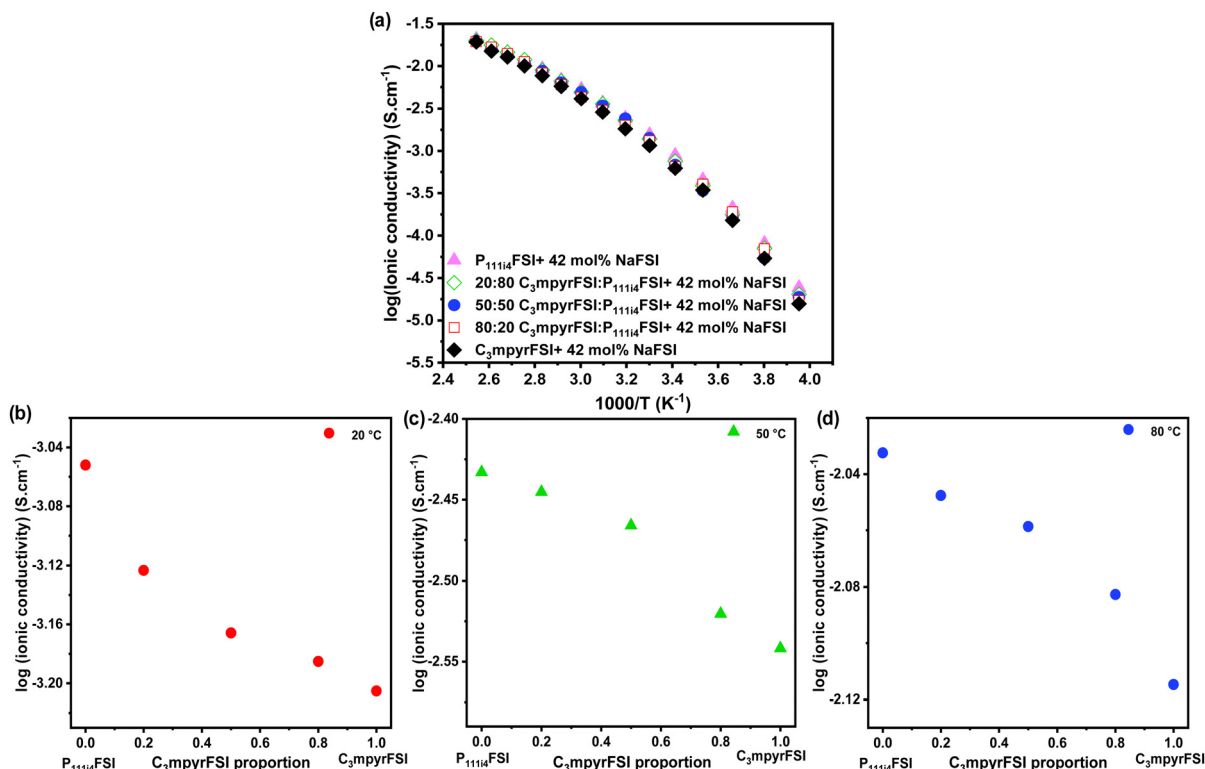
Fig. 6 (a) Temperature-dependent ionic conductivity of the mixed $P_{111i4}FSI$ and $C_3mpyrFSI$ with 42 mol% NaFSI system, (b) the ionic conductivity at 20 °C, (c) the ionic conductivity at 50 °C, (d) the ionic conductivity at 80 °C.

$C_3mpyrFSI$. The glass transition temperature exhibits a linear relationship with the $C_3mpyrFSI$ proportion. However, the observed change is less than 5 °C, indicating a relatively modest impact.
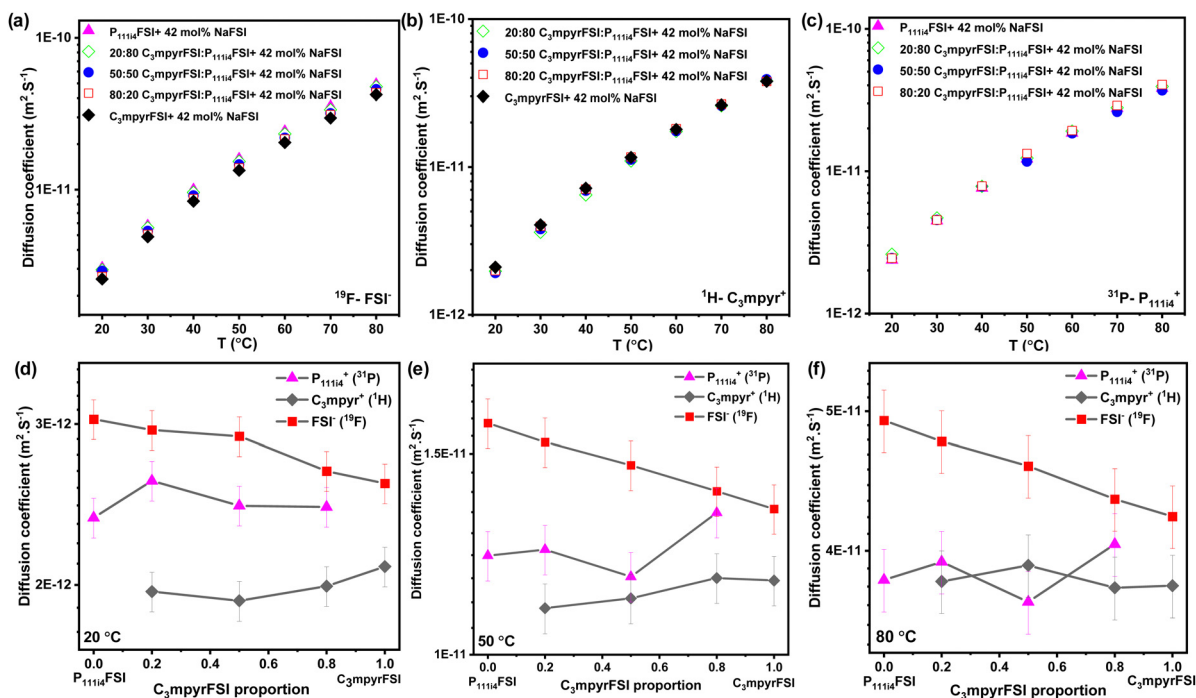

Fig. 7 Diffusion coefficient of (a) anion (^{19}F), (b) C_3mpyr cations (1H), (c) P_{111i4} cations (^{31}P) as a function of $C_3mpyrFSI$ proportion, (d) diffusion coefficients at 20 °C (e) at 50 °C (f) at 80 °C.
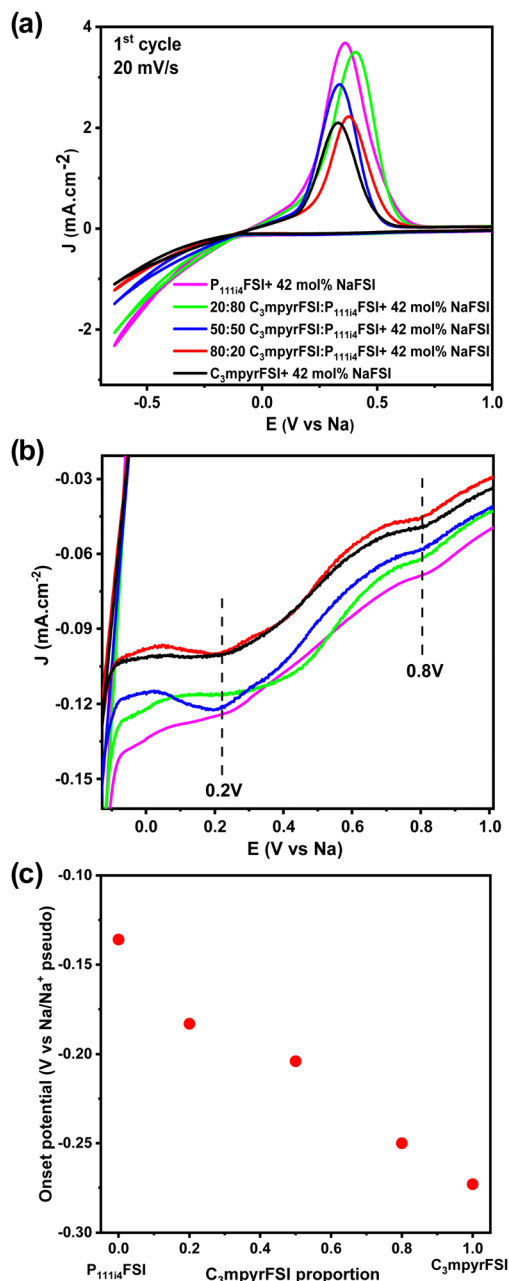
Fig. 8 (a) Cyclic voltammetry curves for the mixed P_{111i4}FSI and C_3mpyrFSI with 42 mol% NaFSI system at 1st cycle, (b) the enlarged reduction process, and (c) the onset potential as a function of C_3mpyrFSI proportion.

Fig. 9 (a) Cyclic voltammetry curves for C_3mpyrFSI + 42 mol% NaFSI from 1st, 2nd and 5th cycle. (b) Coulombic efficiencies as a function of C_3mpyrFSI proportion.

Incorporating P_{111i4}FSI into C_3mpyrFSI/42 mol% NaFSI led to a slight increase in ionic conductivity as shown in Fig. 6. This figure demonstrates a clear linear relationship between the ionic conductivity and the C_3mpyrFSI contents. However, as the temperature increases from −20 to 120 °C (Fig. 6b–d), the increase in ionic conductivity becomes less pronounced. This reduced rate of increase in ionic conductivity could be attributed to factors such as modifications in molecular interactions as temperature rises.

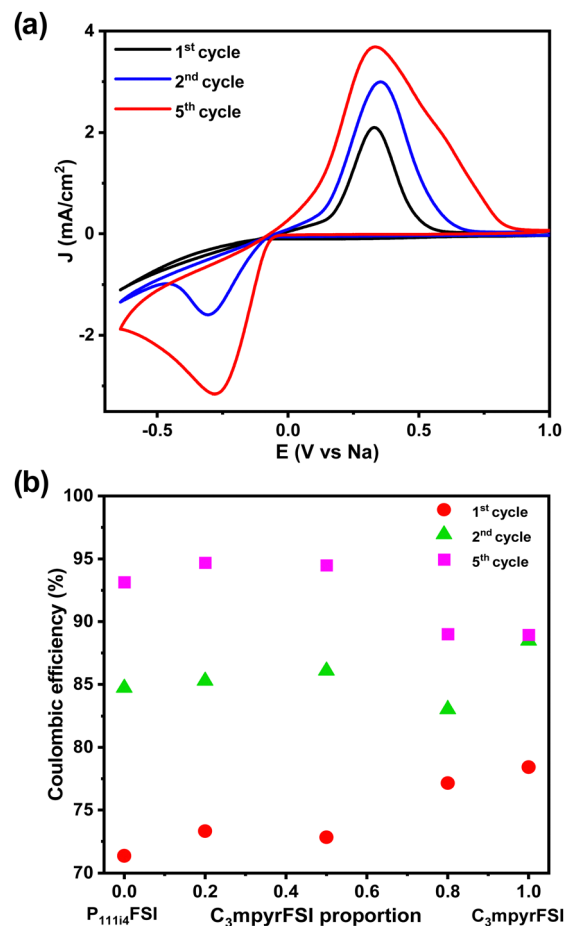**3.2.2. Diffusion coefficient.** Fig. 7 illustrates the diffusion coefficients as a function of the C_3mpyrFSI proportion across the temperature range of 20 to 80 °C. While a slight increase in FSI^- diffusion is observed in Fig. 6a, the changes in the diffusion coefficients of both cations (Fig. 7b and c) are not pronounced. At lower temperatures (Fig. 7d), P_{111i4}^+ exhibits a greater diffusivity than C_3mpyr$^+$, but this difference decreases with rising temperature. Notably, the cation diffusion in mixtures with 42 mol% NaFSI is similar, and the anion diffusion shows a linear relationship with the C_3mpyrFSI proportion. This aligns with the linear trend observed in ionic conductivity.

The findings from the experiments with mixed cations so far indicate that the physicochemical characteristics of the C_3mpyrFSI/42 mol% NaFSI mixture remain largely unaffected by the addition of P_{1111i4}FSI. In the next section, we will explore the electrochemical behaviours of both of the individual ILs/42 mol% NaFSI and their mixtures as electrolytes, using cyclic voltammetry for our analysis.

3.2.3. Cyclic voltammetry. Cyclic voltammetry was employed to characterize the electrochemical properties of the electrolytes. A total of 5 cycles were performed, starting from the open circuit potential to a switching potential at the peak of the reduction potential at −0.64 V (vs. Na). Consistent with our previous reports, electrochemical measurements herein were performed at 50 °C.[16] However, the reproducibility

of the CV curves was poor in the case of the 42 mol% NaFSI system when employing the three-electrode CV setup, despite our best attempts to achieve reproducibility in these flooded systems, as shown in Fig. S5 (ESI†). Therefore, a more practical measurement using a coin cell configuration is utilized instead of three-electrode setup. This is also a more realistic view of how the electrolyte will behave in an actual cell and improved the reproducibility of the CV data, likely attributable to the controlled pressure within the coin cell, promoting the attachment of plated sodium to the working electrode, as well as maintaining a consistent separation distance between the working electrode and the counter electrode.

Fig. 8a shows the comparison of the cyclic voltammetry curves of the different mixtures from the 1st cycle. As the concentration of P_{111i4}FSI increases, changes in the electrochemical behaviour become evident. Specifically, the current density increases, indicating a corresponding decrease in resistance within the system, which may contribute to the high ionic conductivity in the bulk, charge transfer and SEI on the electrode surface. It is worth noting that before the sodium plating (Fig. 8b), two distinct cathodic peaks were observed in all 42 mol% NaFSI system. The peak at 0.2 V corresponds to the decomposition of the FSI^- anion, while the peak at 0.8 V is strongly dependent on the substrate and water content.[27] The increasing onset potential, as depicted in Fig. 8c, indicates that sodium plating initiates earlier with higher P_{111i4}FSI content, *i.e.*, sodium is more easily plated in higher P_{111i4}FSI content systems.

Fig. 9a shows, a comparison of the 1st, 2nd, and 5th cycles for C_3mpyrFSI + 42 mol% NaFSI highlighting an increase in onset potential from -0.27 V in the 1st cycle to -0.048 V in the 3rd cycle. This suggests that sodium is more easily plated over successive cycles. Additionally, the slope of the CV curve on plating sodium becomes sharper with cycling, suggesting an accelerated rate of sodium deposition. Following the sharp increase, there is a subsequent decrease in current density, which may be attributed to the complete utilization of sodium ions on the electrode surface, resulting in a decline in the rate of sodium deposition. Fig. 9b shows with increasing cycle number, the coulombic efficiency increases with cycling. This behaviour could be related to the formation of solid electrolyte interface film on the electrode that is usually formed during the first charge cycle.[7,28] Notably, the C_3mpyr and P_{111i4} CE values exhibit a reverse trend with cycling, with C_3mpyr showing the highest 1st cycle CE value (78%) and the lowest in the 3rd cycle (89%) with the opposite occurring for the higher P_{111i4} compositions (P_{111i4}FSI 1st cycle 71% and 3rd cycle 93%). This suggests more substantial and complete SEI formation in the 1st cycles when the P_{111i4} cation is introduced compared to less substantial and complete SEI formation for the C_3mpyrFSI dominant compositions, which achieve lower efficiency overall.

4. Conclusions

This study focused on exploring the impact of mixed cations on the physicochemical properties of electrolytes using both saturated and fixed NaFSI concentration systems. In the saturated system, we observed significant changes in thermal behaviour and ionic conductivity even though the salt content variation was not particularly high. The addition of NaFSI disrupted the crystallization process in ILs and resulted in an increase in T_g with higher C_3mpyrFSI contents. Additionally, diffusion coefficients for both cations and anions showed consistent increases with elevated P_{111i4}FSI content and higher temperature, corresponding to the rise in T_g and ionic conductivity. Notably, a drop in the diffusion coefficient of C_3mpyr/NaFSI at 20 °C was observed.

In the fixed 42 mol% NaFSI system, we found that T_g slightly decreased with increasing P_{111i4}FSI content. However, the observed change was less than 5 °C, indicating a modest impact. Similarly, the addition of P_{111i4}FSI to C_3mpyrFSI/42 mol% NaFSI led to a slight increase in ionic conductivity, showing a linear relationship with the C_3mpyrFSI ratio. In terms of diffusion, while there was a slight increase in FSI-diffusion, changes in cation diffusion coefficients were not pronounced. Notably, the CV analysis revealed changes in electrochemical behaviour with increasing P_{111i4}FSI content, including an elevated onset potential for sodium plating and changes in current density and coulombic efficiency over cycling, suggesting an accelerated rate of sodium deposition followed by a decline in deposition rate. This work suggests that the approach of mixing IL cations to control physicochemical properties and electrochemical behaviour is feasible and future work will investigate the effect of different cation chemistries. A more detailed study of the electrochemical cycling behaviour in these mixed IL systems is also currently underway.

Author contributions

The manuscript was written through the contributions of all authors. All authors have approved the final version of the manuscript. L. H. – experimental design, methodology, investigation, data analysis, writing original draft. F. M. – supervising, scientific discussion and understanding concept. L. A. O – NMR supervision and scientific discussion. P. H. – conceptualization, supervising, scientific discussion and understanding concept. M. F. – conceptualization, supervising, scientific discussion and understanding concept.

Data availability

^{1}H spectra in NMR, cyclic voltammetry curves for the saturated system, repeated mixtures, and 2nd cycle studied in this work.

Conflicts of interest

The authors declare no conflict of interest.

Acknowledgements

References

1 Y. Hu, X. Zhu and L. Wang, Two-Dimensional Material-Functionalized Separators for High-Energy-Density Metal-Sulfur and Metal-Based Batteries, *ChemSusChem*, 2020, **13**(6), 1366–1378.

2 X. Zhu and L. Wang, Advances in materials for all-climate sodium-ion batteries, *EcoMat*, 2020, **2**(3), e12043.

3 K. Matsumoto, J. Hwang, S. Kaushik, C.-Y. Chen and R. Hagiwara, Advances in sodium secondary batteries utilizing ionic liquid electrolytes, *Energy Environ. Sci.*, 2019, **12**(11), 3247–3287.

4 D. Kundu, E. Talaie, V. Duffort and L. F. Nazar, The emerging chemistry of sodium ion batteries for electrochemical energy storage, *Angew. Chem., Int. Ed.*, 2015, **54**(11), 3431–3448.

5 V. Palomares, P. Serras, I. Villaluenga, K. B. Hueso, J. Carretero-González and T. Rojo, Na-ion batteries, recent advances and present challenges to become low cost energy storage systems, *Energy Environ. Sci.*, 2012, **5**(3), 5884–5901.

6 A. Ponrouch, D. Monti, A. Boschin, B. Steen, P. Johansson and M. R. Palacín, Non-aqueous electrolytes for sodium-ion batteries, *J. Mater. Chem. A*, 2015, **3**(1), 22–42.

7 G. G. Eshetu, G. A. Elia, M. Armand, M. Forsyth, S. Komaba, T. Rojo and S. Passerini, Electrolytes and Interphases in Sodium-Based Rechargeable Batteries: Recent Advances and Perspectives, *Adv. Energy Mater.*, 2020, **10**(20), 2000093.

8 T. Nestler, E. Roedern, N. F. Uvarov, J. Hanzig, G. Antonio Elia and M. de Vivanco, Separators and electrolytes for rechargeable batteries: Fundamentals and perspectives, *Phys. Sci. Rev.*, 2019, **4**(4), 20170115.

9 K. Dong, X. Liu, H. Dong, X. Zhang and S. Zhang, Multiscale Studies on Ionic Liquids, *Chem. Rev.*, 2017, **117**(10), 6636–6695.

10 S. Cha and D. Kim, Anion exchange in ionic liquid mixtures, *Phys. Chem. Chem. Phys.*, 2015, **17**(44), 29786–29792.

11 Z. Xue, L. Qin, J. Jiang, T. Mu and G. Gao, Thermal, electrochemical and radiolytic stabilities of ionic liquids, *Phys. Chem. Chem. Phys.*, 2018, **20**(13), 8382–8402.

12 C. Ding, T. Nohira, K. Kuroda, R. Hagiwara, A. Fukunaga, S. Sakai, K. Nitta and S. Inazawa, NaFSA–C1C3pyrFSA ionic liquids for sodium secondary battery operating over a wide temperature range, *J. Power Sources*, 2013, **238**, 296–300.

13 M. Forsyth, H. Yoon, F. Chen, H. Zhu, D. R. MacFarlane, M. Armand and P. C. Howlett, Novel Na+ Ion Diffusion Mechanism in Mixed Organic–Inorganic Ionic Liquid Electrolyte Leading to High Na+ Transference Number and Stable, High Rate Electrochemical Cycling of Sodium Cells, *J. Phys. Chem. C*, 2016, **120**(8), 4276–4286.

14 F. Chen, P. Howlett and M. Forsyth, Na-Ion Solvation and High Transference Number in Superconcentrated Ionic Liquid Electrolytes: A Theoretical Approach, *J. Phys. Chem. C*, 2018, **122**(1), 105–114.

15 K. Matsumoto, Y. Okamoto, T. Nohira and R. Hagiwara, Thermal and Transport Properties of $Na[N(SO_2F)_2]$– [N-Methyl-N-propylpyrrolidinium]$[N(SO_2F)_2]$ Ionic Liquids for Na Secondary Batteries, *J. Phys. Chem. C*, 2015, **119**(14), 7648–7655.

16 M. Hilder, P. C. Howlett, D. Saurel, E. Gonzalo, A. Basile, M. Armand, T. Rojo, M. Kar, D. R. MacFarlane and M. Forsyth, The effect of cation chemistry on physicochemical behaviour of superconcentrated NaFSI based ionic liquid electrolytes and the implications for Na battery performance, *Electrochim. Acta*, 2018, **268**, 94–100.

17 D. A. Rakov, F. Chen, S. A. Ferdousi, H. Li, T. Pathirana, A. N. Simonov, P. C. Howlett, R. Atkin and M. Forsyth, Engineering high-energy-density sodium battery anodes for improved cycling with superconcentrated ionic-liquid electrolytes, *Nat. Mater.*, 2020, **19**(10), 1096–1101.

18 S. A. Ferdousi, L. A. O'Dell, J. Sun, Y. Hora, M. Forsyth and P. C. Howlett, High-Performance Cycling of Na Metal Anodes in Phosphonium and Pyrrolidinium Fluoro(sulfonyl)imide Based Ionic Liquid Electrolytes, *ACS Appl. Mater. Interfaces*, 2022, **14**(13), 15784–15798.

19 M. Forsyth, M. Hilder, Y. Zhang, F. Chen, L. Carre, D. A. Rakov, M. Armand, D. R. Macfarlane, C. Pozo-Gonzalo and P. C. Howlett, Tuning Sodium Interfacial Chemistry with Mixed-Anion Ionic Liquid Electrolytes, *ACS Appl. Mater. Interfaces*, 2019, **11**(46), 43093–43106.

20 E. M. Barsoukov and J. R. Macdonald, *Impedance Spectroscopy Theory Experiment And Applications*, 2004.

21 P. M. Bayley, G. H. Lane, N. M. Rocher, B. R. Clare, A. S. Best, D. R. MacFarlane and M. Forsyth, Transport properties of ionic liquid electrolytes with organic diluents, *Phys. Chem. Chem. Phys.*, 2009, **11**(33), 7202–7208.

22 S. A. Ferdousi, M. Hilder, A. Basile, H. Zhu, L. A. O'Dell, D. Saurel, T. Rojo, M. Armand, M. Forsyth and P. C. Howlett, Water as an Effective Additive for High-Energy-Density Na Metal Batteries? Studies in a Superconcentrated Ionic Liquid Electrolyte, *ChemSusChem*, 2019, **12**(8), 1700–1711.

23 G. M. A. Girard, M. Hilder, H. Zhu, D. Nucciarone, K. Whitbread, S. Zavorine, M. Moser, M. Forsyth, D. R. Macfarlane and P. C. Howlett, Electrochemical and physicochemical properties of small phosphonium cation ionic liquid electrolytes with high lithium salt content, *Phys. Chem. Chem. Phys.*, 2015, **17**(14), 8706–8713.

24 H. Yoon, H. Zhu, A. Hervault, M. Armand, D. R. Macfarlane and M. Forsyth, Physicochemical properties of N-propyl-N-methylpyrrolidinium bis(fluorosulfonyl)imide for sodium metal battery applications, *Phys. Chem. Chem. Phys.*, 2014, **16**(24), 12350–12355.

25 J. J. Moura Ramos, C. A. M. Afonso and L. C. Branco, Glass transition relaxation and fragility in two room temperature ionic liquids, *J. Therm. Anal. Calorim.*, 2003, **71**, 659–666.

26 A. Basile, F. Makhlooghiazad, R. Yunis, D. R. MacFarlane, M. Forsyth and P. C. Howlett, Extensive Sodium Metal Plating

and Stripping in a Highly Concentrated Inorganic−Organic Ionic Liquid Electrolyte through Surface Pretreatment, *ChemElectroChem*, 2017, **4**(5), 986–991.

27 P. C. Howlett, E. I. Izgorodina, M. Forsyth and D. R. MacFarlane, Electrochemistry at Negative Potentials in Bis(trifluoromethanesulfonyl)amide Ionic Liquids, *Z. Phys. Chem.*, 2006, **220**(10), 1483–1498.

28 Z. W. Seh, J. Sun, Y. Sun and Y. Cui, A Highly Reversible Room-Temperature Sodium Metal Anode, *ACS Cent. Sci.*, 2015, **1**(8), 449–455.